0026-895X/07/7105-1312–1318$20.00
MOLECULAR PHARMACOLOGY
Copyright © 2007 The American Society for Pharmacology and Experimental Therapeutics
Mol Pharmacol 71:1312–1318, 2007

Vol. 71, No. 5
33092/3203977
Printed in U.S.A.

Agonist-Driven Conformational Changes in the Inner β-Sheet of α7 Nicotinic Receptors

James T. McLaughlin, Jie Fu, and Robert L. Rosenberg

Departments of Pharmacology (J.T.M., J.F., and R.L.R.) and Cell & Molecular Physiology (R.L.R.), University of North Carolina at Chapel Hill, Chapel Hill, North Carolina

Received November 28, 2006; accepted February 23, 2007

ABSTRACT

Cys-loop ligand-gated ion channels assemble as pentameric proteins, and each monomer contributes two structural elements: an extracellular ligand-binding domain (LBD) and a transmembrane ion channel domain. Models of receptor activation include rotational movements of subunits leading to opening of the ion channel. We tested this idea using substituted cysteine accessibility to track conformational changes in the inner β sheet of the LBD. Using a nondesensitizing chick α7 background ($L^{247}T$), we constructed 18 consecutive cysteine replacement mutants (Leu^{36} to Ile^{53}) and tested each for expression of acetylcholine (ACh)-evoked currents and functional sensitivity to thiol modification. We measured rates of modification in the presence and absence of ACh to identify conformational changes associated with receptor activation. Resting modification rates of eight substituted cysteines in the β1 and β2 strands and the sequence between them (loop 2) varied over several orders of magnitude, suggesting substantial differences in the accessibility or electrostatic environment of individual side chains. These differences were in general agreement with structural models of the LBD. Eight of 18 cysteine replacements displayed ACh-dependent changes in modification rates, indicating a change in the accessibility or electrostatic environment of the introduced cysteine during activation. We were surprised that the effects of agonist exposure were difficult to reconcile with rotational models of activation. Acetylcholine reduced the modification rate of $M^{40}C$ but increased it at $N^{52}C$ despite the close physical proximity of these residues. Our results suggest that models that depend strictly on rigid-body rotation of the LBD may provide an incomplete description of receptor activation.

Nicotinic acetylcholine receptors are members of the Cys-loop gene family, a group that also includes $GABA_A$, glycine, and $5\text{-}HT_3$ ionotropic receptors. Cys-loop receptors convert the energy of ligand binding into conformational changes that lead to the opening of transmembrane ion channels (Karlin, 2002). The genes in this family encode bifunctional polypeptides that include both an extracellular ligand binding domain (LBD) and a transmembrane ion channel domain (TMD). These receptors also share a similar quaternary structure of homologous or identical polypeptides assembled as a pentamer around a central pore.

The two major structural elements of these receptors are the ligand binding site and the ion channel. The ligand binding site is located at the interface between two receptor subunits ~30 Å from the membrane. It is formed by a set of conserved aromatic residues positioned "beneath" a flexible loop (the C loop) containing ~15 amino acids (Sine, 2002). The central pore of the receptor contains both the ion permeation pathway and the "gate" that controls ion flow. This pore is lined by the second transmembrane helix (M2) from each subunit (Karlin, 2002). The coupling of agonist binding to the opening of the transmembrane ion channel must involve conformational linkage between these two domains. The functional and sequence homology between members of the family suggests that there may also be a common mechanism underlying the linkage between ligand binding and channel gating (Xiu et al., 2005; Sine and Engel, 2006).

Knowledge of the atomic-scale structure of Cys-loop receptors was first obtained from cryoelectron microscopy of AChR from *Torpedo* species electric organ (Unwin, 1993). The X-ray crystal structures of several invertebrate ACh binding proteins (AChBPs) have provided a structural basis for a wealth of biochemical and mutagenesis data (Brejc et al., 2001). The AChBPs exhibit sequence homology to the Cys-Loop LBD, and cocrystals formed with nicotinic agonists or antagonists have confirmed their value in modeling receptor structure

This work was funded by National Institute on Drug Abuse grant DA017882 (to R.L.R.).
Article, publication date, and citation information can be found at http://molpharm.aspetjournals.org.
doi:10.1124/mol.106.033092.

ABBREVIATIONS: 5-HT, 5-hydroxytryptamine; LBD, ligand binding domain; TMD, transmembrane ion channel domain; AChBP, acetylcholine binding protein; SCAM, substituted-cysteine accessibility method; MTSEA, methanethiosulfonate ethylammonium; AChR, acetylcholine receptor; ACh, acetylcholine; ESLC, extracellular solution containing a reduced Ca^{2+} concentration.

based upon a functional homology (Celie et al., 2004; Hansen et al., 2005). Although the AChBPs lack a TMD, Unwin and colleagues (Unwin et al., 2002; Miyazawa et al., 2003; Unwin, 2005) used the high resolution of the AChBP X-ray data to refine their models of *Torpedo* species AChR. Using refined cryoimages of AChRs, they proposed a gating mechanism in which agonist binding leads to rotation of the LBD, particularly in the area of the inner β sheets. They suggest that this rotation is coupled to movements of the M2 transmembrane helix and opening of the ion channel.

Coupling of conformational changes in the LBD to those in the TMD is likely to involve segments positioned at the interface between the LBD domain and the TMD, including loop 2, loop 7, loop 9, pre-M1, and the M2-M3 linker segment (Bouzat et al., 2004; Chakrapani et al., 2004). Salt bridges and salt-bridge switches may be involved in several steps in the activation process (Lee and Sine, 2005; Mukhtasimova et al., 2005). There are conformational linkages between loop 2 and the M2-M3 linker in α7 AChRs (Sala et al., 2005) or between loop 2, loop 7, and the M2-M3 linker in $GABA_A$ receptors (Kash et al., 2003). *Cis-trans* isomerization of a proline in the M2-M3 linker of 5-HT3 receptors provides addition evidence that this segment is a crucial gating element (Lummis et al., 2005). However, many of the specific residues implicated in these studies are not conserved throughout the Cys-loop family, suggesting that there may not be one universal activation mechanism. A consensus gating mechanism has yet to emerge.

Is subunit rotation required for receptor activation? We previously used the substituted-cysteine accessibility method (SCAM) (Karlin and Akabas, 1998) to examine agonist-driven movements in α7 AChRs in loop 9 and obtained results that were consistent with an agonist-induced asymmetric rotation of the LBD (Lyford et al., 2003). In this report, we use the same approach to examine conformational changes in the inner β sheet of the LBD, focusing on loop 2 and surrounding residues in the β1 and β2 strands (Leu^{36} to Ile^{53}). Based upon current models, loop 2 extends into the subunit-subunit interface from the principal binding subunit (+), whereas the β1 and β2 segments line the lower interface of the complementary subunit (−). Using SCAM, we find that side-chain modification rates are generally consistent with the predictions of the structural models. We also find, however, that agonist-dependent changes of modification rates are not consistent with simple rigid-body rotational models of receptor activation.

Materials and Methods

Reagents. Methanethiosulfonate ethylammonium (MTSEA) was obtained from Toronto Research Chemical (Toronto, ON, Canada). Gentamicin was from Invitrogen (Carlsbad, CA). All other reagents were obtained from Sigma-Aldrich (St. Louis, MO).

Site-Directed Mutagenesis. A cDNA clone of the chick α7 receptor containing two mutations ($C^{115}A$, $L^{247}T$) was used as the parental phenotype for mutations described in this study. We mutated the lone unpaired cysteine in the extracellular domain (Cys^{115}) to allow more straightforward interpretation of MTSEA exposure experiments. We observed no functional effect of this mutation on receptor expression or ACh response. We included the mutation of leucine 247 in the M2 transmembrane domain ($L^{247}T$; L9′T) because of its large current amplitudes and nondesensitizing kinetics compared with wild-type α7 receptors (Revah et al., 1991). Mutation at the L9′ position enhances our ability to measure modification kinetics for cysteine replacements in which the ACh-evoked current amplitudes are attenuated (Beene et al., 2002). All mutations were introduced by site-directed mutagenesis using the QuikChange method (Stratagene, La Jolla, CA) as described previously (Eddins et al., 2002) and were confirmed by DNA sequencing.

***Xenopus laevis* Oocyte Maintenance and Expression.** Oocytes were surgically removed and prepared from female *X. laevis* frogs in accordance with UNC Institutional Animal Care and Use Committee guidelines. cRNA was prepared using the T7 RNA polymerase and mMessage mMachine kit as described by the manufacturer (Ambion, Austin, TX). Oocytes were injected with 20 ng of cRNA and incubated at 18°C in ND96 (96 mM NaCl, 2 mM KCl, 1 mM $MgCl_2$, 1.8 mM $CaCl_2$, and 5 mM HEPES, pH 7.5) for 2 to 5 days before use.

Data Collection and Analysis. Oocytes were superfused in normal extracellular solution containing a reduced Ca^{2+} concentration (ESLC; 96 mM NaCl, 2 mM KCl, 1 mM $MgCl_2$, 0.1 mM $CaCl_2$, and 10 mM HEPES, pH 7.5). This solution minimized Ca^{2+} influx and eliminated Ca^{2+}-activated chloride currents. Two-electrode voltage clamp was performed with a GeneClamp 500B controlled by pClamp6 software (Molecular Devices, Sunnyvale, CA). Electrodes

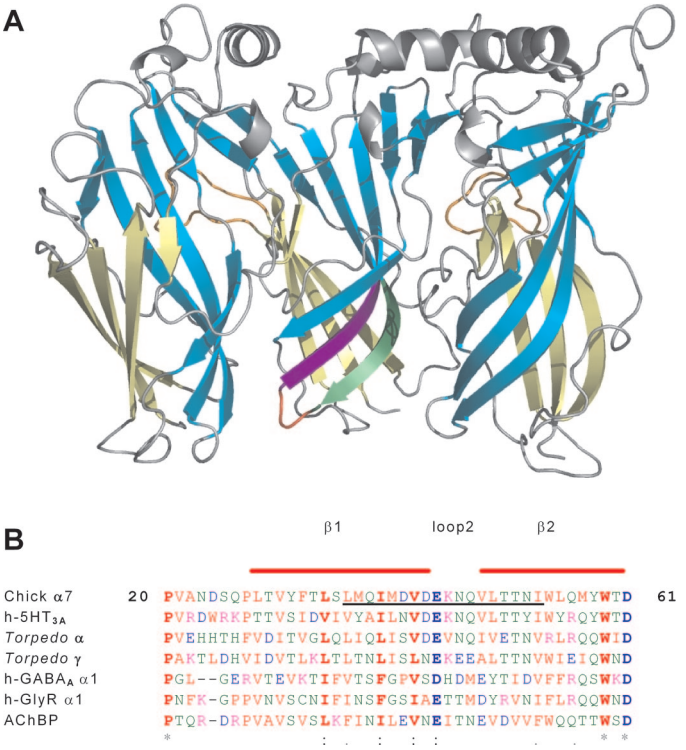

Fig. 1. Structure and sequence of the chick α7 AChR inner β sheet. A, model of the extracellular domain. For simplicity, two of the five subunits are omitted. The view is from the inside of the extracellular vestibule. The inner (cyan) and outer (yellow) β sheets are highlighted in the three subunits shown. The C loops (orange) are located behind the subunits in this view. Residues targeted for SCAM are shown in the center subunit; the lower half of β1 (Leu^{36}–Asp^{43}) is green, loop 2 (Glu^{44}–Gln^{47}) is red, and the lower half of β2 (Val^{48}–Ile^{53}) is purple. Note that the loop 2 residues extend into the subunit-subunit interface from the principal binding subunit (left interface of the center subunit), whereas the β1 and β2 segments line the vestibule and the lower interface of the complementary subunit (right interface). B, sequence alignment of β1-loop2-β2 region of cys-loop receptors. This region includes three residues that are absolutely conserved in all cys-loop receptors (starred positions) and four others that show relative conservation, including Ile^{39} and Glu^{44}. The portion of β1 that shows the highest degree of conservation (Leu^{34}–Glu^{44}) forms part of the subunit-subunit interface in the ACh binding proteins (Brejc et al., 2001). Residues underlined were included in this cysteine scanning study.

were filled with 3 M KCl contacting Ag-AgCl wires and had resistances of 0.5 to 2.0 MΩ. Currents were recorded at a constant holding potential of −60 mV. Currents were low pass-filtered at 50 Hz and sampled at 100 Hz. Agonist dose-response curves were obtained as described previously (Eddins et al., 2002), and data were fit to the Hill equation using Origin software (OriginLab Corp, Northampton, MA).

Expression and Modification Kinetics. Each mutant was initially screened for functional expression over a range of ACh concentrations to generate a dose-response relationship and determine its EC_{50}. To test for reactivity of introduced free thiols, we compared responses of each mutant to an ~EC_{50} ACh dose before and after exposure to high concentrations of MTSEA (0.5–1.0 mM) applied by continuous flow for 30 to 60 s. MTSEA was prepared daily in distilled water and stored on ice. Stock solution was diluted to the appropriate working concentration in ESLC immediately before each application. In some cases ($Q^{47}C$, $N^{52}C$), the effect of modification at saturating MTSEA concentrations was accelerated by the presence of ACh. For these mutants, the maximal effect of MTSEA was obtained by coapplication of MTSEA and ACh or by prolonged exposure to MTSEA in the absence of ACh. For mutants that displayed a functional effect of MTSEA, we determined a limiting dose of modifier; oocytes were exposed to low concentrations of MTSEA (0.1–100 μM) for 15 to 30 s and then challenged with a submaximal concentration of ACh. A limiting dose, yielding 20 to 40% of the maximal MTSEA effect, was identified for each mutant and used to measure modification kinetics. Kinetic data were analyzed as described previously (Pascual and Karlin, 1998).

Structural Model of α7. A model of the chick α7 nicotinic receptor extracellular domain, based on the coordinates of the *Lymnea* ACh binding protein (Brejc et al., 2001) was constructed as described previously (Lyford et al., 2003; McLaughlin et al., 2006). Images of the model were generated with Pymol (DeLano Scientific, South San Francisco, CA). Distance estimates between amino acids were made using β carbons as a reference point. We estimated the position of the ACh binding using the β carbon of the principal (+) subunit Trp^{148}, the central conserved residue in the aromatic ligand binding pocket (Sine, 2002). We also used a model of the full-length human α7 AChR for some of our analysis; coordinates for this model were generously provided by Dr. A. Taly (Université Louis Pasteur, Strasbourg, France).

Results

A prominent feature of the α7 LBD is a pair of β sheets, the inner and outer sheets, that constitute ~60% of the LBD mass and have been implicated in conformational movements accompanying receptor activation (Brejc et al., 2001; Unwin et al., 2002). The inner sheet also includes loop 2, the linker sequence between β-strands 1 and 2 that is involved in linkage between the LBD and the TMD (Kash et al., 2003; Chakrapani et al., 2004; Lee and Sine, 2005; Sala et al., 2005). To examine conformational changes in the inner sheet, we constructed a series of 18 consecutive single cysteine replacement mutations from Leu^{36} to Ile^{53}. This region includes loop 2 and portions of the flanking β1 and β2 strands (Fig. 1). Fourteen of 18 mutations exhibited acetylcholine-evoked currents when expressed in *X. laevis* oocytes. Four mutants failed to show ACh-evoked currents: a pair of adjacent residues, $Q^{38}C/I^{39}C$, and two leucines, $L^{36}C$ and $L^{49}C$. Of the mutations that expressed functional currents, most had peak currents comparable with the parental phenotype ($C^{115}A/L^{247}T$: EC_{50}, 2.3 μM; I_{max}, ~0.5–5 μA; summarized in Table 1). The exceptions were $D^{41}C$, $N^{46}C$, and $T^{50}C$, which exhibited substantially reduced peak currents (I_{max}~40 nA). Large effects of Cys replacements on ACh-evoked responses were localized to loop 2 ($D^{43}C$ to $Q^{47}C$), a region known to play a role in the gating process (Kash et al., 2003; Chakrapani et al., 2004; Lee and Sine, 2005).

We next examined the susceptibility of the introduced cysteines to chemical modification by measuring dose-responses to ACh before and after exposure to the thiol modifier MTSEA. The goal of these experiments was to identify the cysteines that could be used as reporters for agonist-induced conformational changes. An example of this analysis, using the $M^{40}C$ mutation as an example, is shown in Fig. 2. After exposure to MTSEA (10 μM, 30 s) the ACh-evoked dose-response curve was shifted to the right and the EC_{50} was increased from 2.3 to 36 μM, demonstrating that the introduced thiol group was accessible to the aqueous modifying reagent. When the same MTSEA exposure was done in the

TABLE 1

Properties of α 7 AChR cysteine mutants of the β 1-loop2-β 2 region

The EC_{50} and I_{max} measurements for each receptor mutation represent mean values (± S.E.M.) from at least three separate experiments. For dose-response relationships that did not reach a plateau, EC_{50} and I_{max} values represent a lower limit. Mutants that had an MTSEA effect (indicated by +) had a statistically significant different EC_{50} after MTSEA exposure (paired *t* test, $P < 0.05$).

Mutant	Before MTSEA Exposure		MTSEA Effect?	After MTSEA Exposure			Modification Rate	
	ACh EC_{50}	I_{max}		ACh EC_{50}	I_{max}	I_{max} (of control)	−ACh	+ ACh
	μM	μA		μM	μA	%	$M^{-1}s^{-1}$ (*n*)	
$C^{115}A/L^{247}T$	2.4 ± 0.1	5.0 ± 0.7	−					
$M^{37}C$	2.3 ± 0.3	0.4 ± 0.2	+	>1000[a]	0.05 ± 0.03[a]	13[a]	$4.7 \pm 1.1 \times 10^3$ (8)	$6.3 \pm 1.3 \times 10^2$ (5)
$M^{40}C$	2.6 ± 0.4	1.5 ± 0.3	+	22 ± 5.8	1.3 ± 0.4	87	$2.7 \pm 0.8 \times 10^4$ (6)	$3.2 \pm 0.8 \times 10^3$ (4)
$D^{41}C$	9.1 ± 2.0	0.04 ± 0.01	−					
$V^{42}C$	7.7 ± 0.4	1.0 ± 0.3	+	46 ± 11	0.7 ± 0.4	70	$1.2 \pm 0.4 \times 10^2$ (3)	$1.6 \pm 0.7 \times 10^1$ (4)
$D^{43}C$	46 ± 3.4	0.5 ± 0.1	+	54 ± 4.4	0.5 ± 0.2	100	$3.5 \pm 0.4 \times 10^1$ (3)	$7.1 \pm 0.9 \times 10^1$ (3)
$E^{44}C$	12 ± 1.3	5.6 ± 0.7	+	27 ± 1.0	4.9 ± 0.08	88	$6.3 \pm 2.4 \times 10^4$ (7)	$4.9 \pm 1.1 \times 10^3$ (4)
$K^{45}C$	71 ± 22	3.5 ± 0.2	+	45 ± 7.3	3.5 ± 0.4	100	$2.1 \pm 5.3 \times 10^4$ (5)	$5.9 \pm 1.1 \times 10^4$ (4)
$N^{46}C$	15 ± 0.6	0.04 ± 0.01	−					
$Q^{47}C$	60 ± 11	1.5 ± 0.1	+	39 ± 7.6	1.2 ± 0.1	80	$2.5 \pm 1.2 \times 10^1$ (5)	$1.0 \pm 0.2 \times 10^3$ (6)
$V^{48}C$	11 ± 2.1	4.1 ± 0.9	−					
$T^{50}C$	9.3 ± 0.4	0.03 ± 0.01	−					
$T^{51}C$	4.3 ± 0.3	1.3 ± 0.5	−					
$N^{52}C$	13 ± 3.0	0.4 ± 0.2	+	>1000[a]	0.02 ± 0.01[a]	5[a]	$6.8 \pm 3.5 \times 10^1$ (4)	$1.7 \pm 0.3 \times 10^3$ (3)
$I^{53}C$	1.6 ± 0.1	5.1 ± 0.6	−					

[a] Dose-response relationships that did not reach a plateau.

presence of a saturating concentration of ACh, however, the shift in dose-response curve was substantially smaller (from 2.3 to 11 μM). Thus, the sensitivity of this residue to thiol modification was agonist-dependent and can therefore be used to test changes in accessibility or electrostatic environment resulting from ACh-induced conformational changes.

Similar analysis of the entire series of Cys mutants identified seven additional substitutions that displayed a functional sensitivity to MTSEA (summarized in Table 1). Significant changes in EC_{50} after MTSEA exposure show that of the 14 receptors that are functionally expressed, at least eight cysteine substitutions in the region between Leu^{36} and Ile^{53} have side chains that are accessible to aqueous solvent. Six mutants (plus the $C^{115}A/L^{247}T$ parental phenotype) exhibited no effect of MTSEA application (Table 1); for these we cannot distinguish between a lack of thiol modification and the lack of a functional effect.

Thiol reactivity can be used to explore conformational changes induced by ACh or other ligands. Such conformational sensitivity is best explored by measuring modification rates under resting and activating conditions. Using repeated application of subsaturating doses of MTSEA it is possible to measure the time- and concentration-dependence of the MTSEA effect. The goal of these modification rate experiments was to detect ACh-induced changes in side-chain modification accessibility or electrostatic environment. Figure 3 shows data from one such experiment, using the $E^{44}C$ mutant as an example. Oocytes were challenged with a test dose of ACh (at a concentration near the EC_{50} for that mutant) between brief exposures to a limiting concentration of MTSEA (Fig. 3A). The sequential decrement in currents elicited by the test dose reflected an increasing fraction of receptors that were modified; the endpoint was established with a longer exposure to a high dose of MTSEA. We compared the time course of this current decay with that from another oocyte challenged with the same limiting MTSEA concentration in the presence of saturating ACh (Fig. 3B). In the case of $E^{44}C$ receptors, ACh caused a decrease in the rate of MTSEA modification, suggesting that conformational changes associated with ACh binding drive the $E^{44}C$ side chain to a less accessible position. Normalized data are plotted (Fig. 3C) to extract a rate constant for the reaction between the AChR and the MTSEA (Table 1). These rate constants provide a means to compare the water accessibility and electrostatic environment of individual residues, as well as the changes in access or environment evoked by ACh binding and activation.

Normalized rate measurements for three additional mutations ($M^{37}C$, $M^{40}C$, and $N^{52}C$) are shown in Fig. 4. Based upon models of the α7 LBD, the side chains of these three positions should extend toward the subunit-subunit interface in close proximity. Despite this proximity, we observed a qualitative difference in the agonist effect on MTSEA modi-

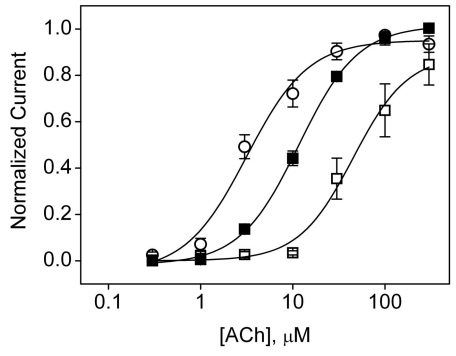

Fig. 2. Functional effects of MTSEA on $M^{40}C$ α7 AChRs. ○, ACh dose-response relationship before exposure to MTSEA (EC_{50} = 2.6 μM); □, ACh dose response after a 30-s exposure to 10 μM MTSEA (EC_{50} = 36 μM); ■, ACh dose response (EC_{50} = 11 μM) after a 30-s exposure to 10 μM MTSEA in the presence of 30 μM ACh. Thus, the effect of MTSEA was attenuated in the presence of ACh. Data are normalized from three determinations.

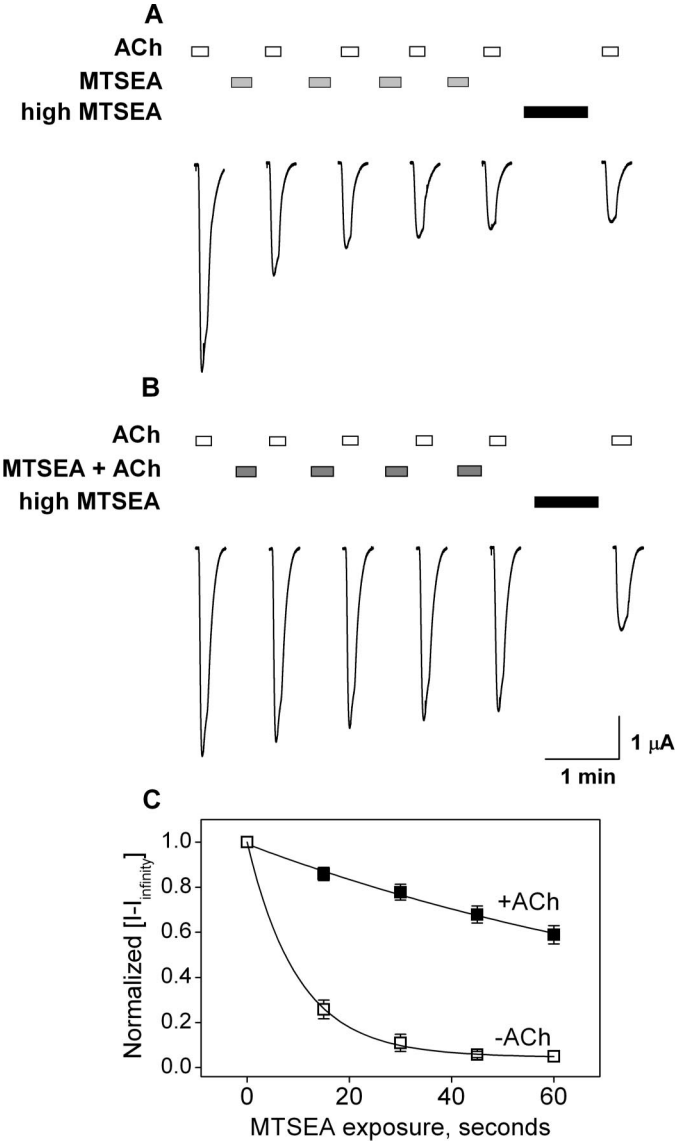

Fig. 3. ACh affects the rate of MTSEA modification. A, ACh-evoked currents (10 μM, open bars) of α7 $E^{44}C$ AChRs were inhibited by repeated exposure to limiting doses of MTSEA (1 μM, 15 s, gray bars). The maximal effect of MTSEA (0.5 mM, 60 s, black bars) was measured after four limited exposures. B, ACh-evoked currents (10 μM, open bars) were less inhibited when repeated limiting MTSEA exposures (1 μM) were in the presence of a saturating ACh concentration (100 μM ACh, gray bars). Current responses elicited by the coapplication of MTSEA and ACh are not shown. C, normalized data of $\{I(t) - I(\infty)\}/\{I(0) - I(\infty)\}$, where I(t) is the current after each exposure to 1 μM MTSEA for cumulative time t, I(0) is the initial current before MTSEA exposure, and I(∞) is the current after the maximal exposure to MTSEA (0.5 mM, 60 sec). Data were obtained in the absence of ACh (■) or in the presence of 100 μM ACh (□). Data are fit to a single exponential decay to derive a pseudo-first-order rate constant for reaction between the $E^{44}C$ side chain and MTSEA.

fication; coapplication of ACh slowed the rate of modification at $M^{37}C$ and $M^{40}C$ but increased the rate at $N^{52}C$. A plot of the rate constants for MTSEA modification in the absence and presence of saturating concentrations of ACh is shown in Fig. 5, and the rate constants are provided in Table 1. Overall, four mutants exhibited a decrease in the rate of modification in the presence of ACh; these mutations are either in the β1 strand or in loop 2 ($M^{37}C$, $M^{40}C$, $V^{42}C$, and $E^{44}C$). In general, these mutants exhibited extremely high MTSEA modification rates (5000–45,000 $M^{-1}s^{-1}$) in the absence of ACh and ~10-fold decreases in modification rates in the presence of ACh. Thus, in the resting conformation, these residues were readily accessible to solvent and were less accessible in the ACh-activated state. At $V^{42}C$, the reaction rate was slow in the absence of ACh (125 $M^{-1}s^{-1}$, ~500 times slower than $E^{44}C$) but also showed a decrease in the presence of ACh, to less than 20 $M^{-1}s^{-1}$.

Modification rates at four other residues were increased in the presence of ACh. At two sites ($Q^{47}C$ and $N^{52}C$), modification rates increased 20- to 40-fold when the MTSEA was coapplied with a saturating dose of ACh. The increase in modification rate in the presence of ACh suggests a movement of these residues from a position of limited accessibility to one of greater accessibility to aqueous solvent. At two additional sites, $D^{43}C$ and $K^{45}C$, we observed a 2- to 3-fold increase in modification rates in the presence of ACh. There is a general trend in which the residues in the β1 strand showed decreased reaction rates during activation, whereas residues in the β2 strand showed increased reaction rates. The implications of these agonist-induced changes of side-chain accessibility or environment are discussed below.

Discussion

The inner and outer β sheets comprise the largest structural elements of the LBD of Cys-loop receptors (Brejc et al., 2001). Conformational transitions underlying ligand-induced activation are likely to involve these structures. In this study, we focused on a key region of the inner β sheet: loop 2 and flanking residues in the β1 and β2 strands. By measuring rates of thiol modification, we assessed the validity of homology-based models of the α7 AChR extracellular domain. In addition, agonist-induced changes in modification rates provided a test of receptor activation models.

Is The Pattern of Cysteine Modification Consistent with Structural Models?

β1 Strand. Structural models (Sine et al., 2002; Lyford et al., 2003; Taly et al., 2005) predict that Met^{37} and Met^{40} are on the (−) face of the subunit-subunit interface and accessible to solvent from the outside or from the vestibule of the receptor, respectively. The side chains of Asp^{41} and Asp^{43} are also predicted to be accessible from vestibule of the receptor. Models predict that Gln^{38} and Ile^{39} are buried at the subunit-subunit interface and that Val^{42} is buried in the subunit core. The high modification rates of $M^{37}C$ and $M^{40}C$ (5000–20,000 $M^{-1}s^{-1}$) establish their surface accessibility, in agreement with structural models. We found poor expression and no significant MTSEA effect at $D^{41}C$, providing inconclusive results. There was a small but significant effect of modification at $D^{43}C$, indicating accessibility of this residue, although the modification rate (30 $M^{-1}s^{-1}$) was lower than predicted by the models that show the side chain projecting toward the vestibule. The modification rate of $V^{42}C$ (125 $M^{-1}s^{-1}$) was also low, suggesting limited accessibility. Overall, our results in the β1 strand suggest that the structural models are valid at most locations, but the data deviate somewhat from the predictions of the models at the C terminus of β1.

Loop 2. The loop connecting the β1 and β2 strands includes Glu^{44}, Lys^{45}, Asn^{46}, and Gln^{47}. The models predict that Glu^{44}, Lys^{45}, and Gln^{47} are accessible from the outside of the receptor and that Asn^{46} is at the subunit-subunit interface and may be accessible from the vestibule. Both $E^{44}C$ and $K^{45}C$ reacted with MTSEA at extremely high rates (>10,000 $M^{-1}s^{-1}$), consistent with a side-chain position that is readily accessible to the aqueous environment. $N^{46}C$ receptors expressed poorly, suggesting that this residue is critical for assembly and/or gating. MTSEA had a small but significant effect on $Q^{47}C$ receptors, also as predicted by models showing this residue to be surface accessible.

The charge at position Glu^{44} is strongly conserved throughout the Cys-loop family (Fig. 1B), and reports have suggested a critical role for this residue in channel gating (Kash et al., 2003; Lee and Sine, 2005). Our result, that $E^{44}C$ α7 receptors express at normal levels with an ACh EC_{50} that is elevated only 5-fold above the parental isoform, argues against a critical role for Glu^{44} in the activation of chick α7 AChRs. The high rates of modification we observe at $K^{45}C$ seem inconsistent with a role for this residue in a "pin-and-socket" mechanism (Miyazawa et al., 2003). Similar conclusions were drawn in cysteine accessibility studies of the aligned residue in 5-HT_3 receptors ($K^{81}C$; Reeves et al., 2005). Instead, our results are more consistent with the idea that different members of the Cys-loop receptor family use different molecular interactions during gating (Xiu et al., 2005).

β2 Strand. Models predict that the side chains of Val^{48}, Thr^{50}, and Asn^{52} are accessible to the aqueous environment

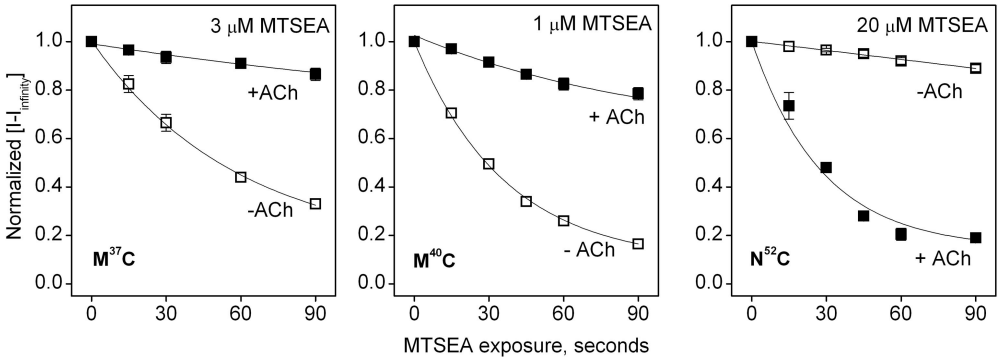

Fig. 4. ACh decreases the rate of MTSEA modification of $M^{37}C$ and $M^{40}C$ but increases the rate of modification of $N^{52}C$. Data were obtained and plotted as described in Fig. 3. The modification rates of each mutant were determined with a limiting dose of MTSEA as indicated.

of the vestibule, whereas those of Leu[49], Thr[51], and Ile[53] are buried in the subunit core. Our results were generally consistent with the predictions of the models. V[48]C and T[50]C exhibited no functional effect of MTSEA exposure, an inconclusive result because a lack of effect of modification is impossible to distinguish from a lack of MTSEA accessibility. N[52]C was accessible to MTSEA, because MTSEA greatly decreased subsequent responses to ACh concentrations up to 3 mM. L[49]C receptors did not express, suggesting a requirement for a hydrophobic side chain at this location. Muscle receptors with a leucine-to-lysine substitution at this position also express poorly (Sine et al., 2002). T[51]C and I[53]C receptors were insensitive to MTSEA, another inconclusive result but one that is consistent with the structural models.

***β1-β2* Bend.** Three substitutions in β1 and β2, including two adjacent residues (Q[38]C, I[39]C, and L[49]C) yielded receptors that were unresponsive to ACh. Both Ile[39] and Leu[49] are conserved in Cys-loop receptors (Brejc et al., 2001). In crystal structures of AChBPs (Brejc et al., 2001, Celie et al., 2004; Hansen et al., 2005) and Cys-loop receptor models (Le Novere et al., 2002; Sine et al., 2002; Lyford et al., 2003; Taly et al., 2005), these residues are at a major bend in the β1-β2 strand. The effect of Cys mutations at these positions may indicate the importance of side-chains required to stabilize this structural element.

Are ACh-Dependent Changes in Cysteine Modification Rates Consistent with Subunit-Rotation Models for Activation?

Modification rate analysis can be used to measure both the degree of side chain accessibility and changes in accessibility or electrostatic environment during receptor activation. Of the eight Cys replacements in which rates of modification were measured, four sites exhibited a protective effect of ACh. At M[37]C, M[40]C, V[42]C, and E[44]C, modification rates decreased 5- to 10-fold in the presence of saturating ACh concentrations. A direct, physical occlusion of modifier accessibility by ACh could explain decreases in modification rate of M[37]C because of its proximity to the ligand-binding pocket. Physical occlusion, however, is less likely to explain the decreased reaction rates of M[40]C, V[42]C, or E[44]C, because models suggest that these side-chains are more than 20 Å from the bound ligand. Instead, ACh is likely to cause reduced modification at these sites because of the conformational changes initiated during receptor activation.

We found that ACh caused an increase in modification rates at four positions: D[43]C, K[45]C, Q[47]C, and N[52]C. At these sites, increased rates must be due to conformational changes associated with receptor activation that increase the access of MTSEA to the introduced thiol groups.

The pattern of modification rates and agonist-driven changes in modification rates provide tests of theoretical models for receptor activation. Unwin and colleagues (Miyazawa et al., 2003; Unwin, 2005) propose a model for activation of *Torpedo* species AChRs in which ACh binding leads to a clockwise rotation of the LBD and TMD of the two α subunits. We have shown that movements around a conserved glutamate in the β8-β9 loop (loop 9) are consistent with rotational models of α7 AChR activation (Lyford et al., 2003).

While the general pattern of ACh effects on modification rates (decreases in β1, increases in β2) might seem compatible with an activation model that involves inner β-sheet rotation, the specific changes in rates we observe at M[37]C, M[40]C, and N[52]C argue against a simple rotation. In each of

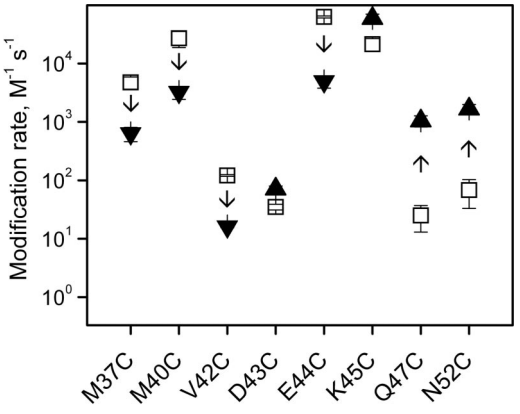

Fig. 5. ACh alters the MTSEA modification rates of most Cys substitutions in the β1-loop2-β2 region. Modification rates were measured in the absence (□) or presence (▲, ▼) of saturating ACh concentrations. ▼, residues in which the modification rates were *decreased* by ACh (M[37]C, M[40]C, V[42]C, E[44]C); ▲, residues in which modification rates were *increased* by ACh (D[43]C, K[45]C, Q[47]C, N[52]C). Rate data from two to four separate determinations are averaged.

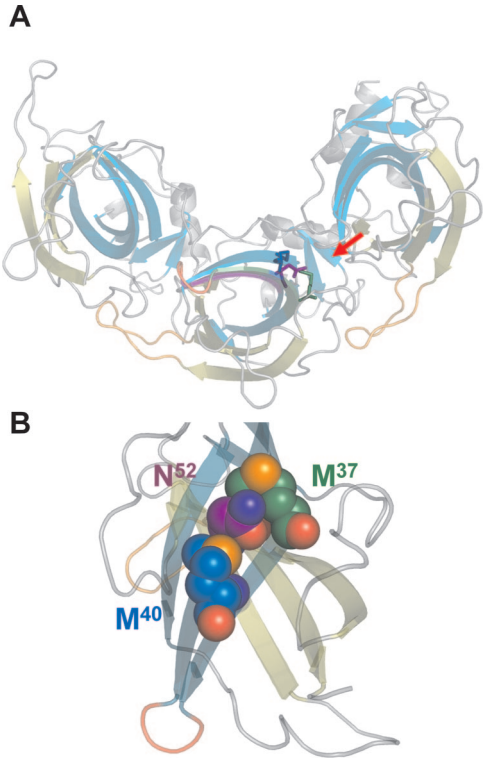

Fig. 6. Alignment of residues Met[37], Met[40], and Asn[52]. A, model of α7 LBD viewed from below. As with Fig. 1, two subunits are omitted for simplicity. Each subunit includes an inner (cyan) and an outer (yellow) β sheet. The C-loops form the outer boundary for the two subunit-subunit interfaces shown. Positions of the three residues on the (−) face of the left interface are shown in stick format: Met[37] (green), Met[40] (blue), and Asn[52] (purple). B, a view of the (−) face, viewed from across the interface (from the arrow in A). A single monomer is shown with the interface between the LBD and TMD (including loop 2, in red) at the bottom. The atoms of Met[37], Met[40], and Asn[52] are shown as spheres to emphasize their proximity. The color scheme for carbon atoms is: Met[37], green; Met[40], blue; Asn[52], purple. Color scheme for other atoms is: nitrogen, dark blue; oxygen, red; sulfur, orange.

these residues, side-chains are exposed to the aqueous cleft on the inner β sheet of the (−) face of the subunit-subunit interface (Fig. 6). The arrangement of the β1 and β2 strands places these side chains in close vertical register, with the Asn^{52} positioned between Met^{37} and Met^{40}. If ACh initiates a rotation of the entire β sheet, we expect that the three residues to undergo a concerted movement and modification rates of all three residues should either increase or decrease. We observed, however, an 8-fold decrease in the modification rates of $M^{37}C$ and $M^{40}C$ but a 25-fold increase in modification rate of $N^{52}C$ (Table 1). It is difficult to reconcile these results with models for ACh activation of nicotinic receptors that that rely on simple rotation of the LBD.

If we presume that the observed changes in modification rates result from multiple conformational perturbations at each site, our results can be brought into line with rotational models. There could be a combination of local (e.g., steric or electrostatic effects of nearby side chains) and global rotational effects that sum to yield a net effect on modification rate. For example, the Asn^{52} residue is near a conserved Trp residue (Trp^{54}) that participates in the "aromatic pocket," forming the ACh-binding site (Xie and Cohen, 2001). If ACh binding moves Trp^{54} away from Asn^{52}, it could relieve steric or electrostatic constraints and increase MTSEA modification of $N^{52}C$. If, at the same time, the entire inner β sheet rotated to a position of reduced modifier accessibility, the net effect could slow modification rates of other inner β sites, such as Met^{37} and Met^{40}, even as the modification rate of Asn^{52} was increased. The difficulty with this idea is magnitude of the rate changes involved. To account for the 25-fold increase in the modification rate of $N^{52}C$, the local effect of Trp^{54} movement would have to specifically increase Asn^{52} modification rate 200-fold to overcome the 8-fold decrease in modification caused by the rigid-body rotation.

Conclusions

Overall, our results are consistent with the structural models of α7 nicotinic receptors derived from the structure of AChBPs. Our results, however, are not consistent with models for receptor activation that rely strictly on rigid-body rotation of the LBD. Instead, our results suggest that a combination of local conformational changes, leveraged movements of β-sheets (McLaughlin et al., 2006) that could cause tilting of transmembrane α-helices (Cheng et al., 2006), and rotation of the TMD relative to the LBD (Law et al., 2005) all may be components of the "conformational wave" (Grosman et al., 2000) that transmits information from the ligand-binding site to the gate of the channel.

References

Beene DL, Brandt GS, Zhong W, Zacharias NM, Lester HA, and Dougherty DA (2002) Cation-π interactions in ligand recognition by serotonergic (5-HT_{3A}) and nicotinic acetylcholine receptors: the anomalous binding properties of nicotine. *Biochemistry* **41:**10262–10269.

Bouzat C, Gumilar F, Spitzmaul G, Wang HL, Rayes D, Hansen SB, Taylor P, and Sine SM (2004) Coupling of agonist binding to channel gating in an ACh-binding protein linked to an ion channel. *Nature (Lond)* **430:**896–900.

Brejc K, van Dijk WJ, Klaassen RV, Schuurmans M, van Der Oost J, Smit AB, and Sixma TK (2001) Crystal structure of an ACh-binding protein reveals the ligand-binding domain of nicotinic receptors. *Nature (Lond)* **411:**269–276.

Celie PH, van Rossum-Fikkert SE, van Dijk WJ, Brejc K, Smit AB, and Sixma TK (2004) Nicotine and carbamylcholine binding to nicotinic acetylcholine receptors as studied in AChBP crystal structures. *Neuron* **41:**907–914.

Chakrapani S, Bailey TD, and Auerbach A (2004) Gating dynamics of the acetylcholine receptor extracellular domain. *J Gen Physiol* **123:**341–356.

Cheng X, Wang H, Grant B, Sine SM, and McCammon JA (2006) Targeted molecular dynamics study of c-loop closure and channel gating in nicotinic receptors. *PLoS Comput Biol* **2:**1173–1184.

Eddins D, Sproul AD, Lyford LK, McLaughlin JT, and Rosenberg RL (2002) Glutamate 172, essential for modulation of $L^{247}T$ alpha7 ACh receptors by Ca^{2+}, lines the extracellular vestibule. *Am J Physiol* **283:**C1454–C1460.

Grosman C, Zhou M, and Auerbach A (2000) Mapping the conformational wave of acetylcholine receptor channel gating. *Nature (Lond)* **403:**773–776.

Hansen SB, Sulzenbacher G, Huxford T, Marchot P, Taylor P, and Bourne Y (2005) Structures of *Aplysia* AChBP complexes with nicotinic agonists and antagonists reveal distinctive binding interfaces and conformations. *EMBO (Eur Mol Biol Organ) J* **24:**3635–3646.

Karlin A (2002) Emerging structure of the nicotinic acetylcholine receptors. *Nat Rev Neurosci* **3:**102–114.

Karlin A and Akabas MH (1998) Substituted-cysteine accessibility method. *Methods Enzymol* **293:**123–145.

Kash TL, Jenkins A, Kelley JC, Trudell JR, and Harrison NL (2003) Coupling of agonist binding to channel gating in the $GABA_A$ receptor. *Nature (Lond)* **421:**272–275.

Law RJ, Henchman RH, and McCammon JA (2005) A gating mechanism proposed from a simulation of a human alpha7 nicotinic acetylcholine receptor. *Proc Natl Acad Sci USA* **102:**6813–6818.

Lee WY and Sine SM (2005) Principal pathway coupling agonist binding to channel gating in nicotinic receptors. *Nature (Lond)* **438:**243–247.

Le Novere N, Grutter T, and Changeux JP (2002) Models of the extracellular domain of the nicotinic receptors and of agonist- and Ca^{2+}-binding sites. *Proc Natl Acad Sci USA* **99:**3210–3215.

Lummis SC, Beene DL, Lee LW, Lester HA, Broadhurst RW, and Dougherty DA (2005) Cis-trans isomerization at a proline opens the pore of a neurotransmitter-gated ion channel. *Nature (Lond)* **438:**248–252.

Lyford LK, Sproul AD, Eddins D, McLaughlin JT, and Rosenberg RL (2003) Agonist-induced conformational changes in the extracellular domain of alpha 7 nicotinic acetylcholine receptors. *Mol Pharmacol* **64:**650–658.

McLaughlin JT, Fu J, Sproul AD, and Rosenberg RL (2006) Role of the outer beta-sheet in divalent cation modulation of α7 nicotinic receptors. *Mol Pharmacol* **70:**16–22.

Miyazawa A, Fujiyoshi Y, and Unwin N (2003) Structure and gating mechanism of the acetylcholine receptor pore. *Nature (Lond)* **423:**949–955.

Mukhtasimova N, Free C, and Sine SM (2005) Initial coupling of binding to gating mediated by conserved residues in the muscle nicotinic receptor. *J Gen Physiol* **126:**23–39.

Pascual JM and Karlin A (1998) State-dependent accessibility and electrostatic potential in the channel of the acetylcholine receptor. Inferences from rates of reaction of thiosulfonates with substituted cysteines in the M2 segment of the alpha subunit. *J Gen Physiol* **111:**717–739.

Reeves DC, Jansen M, Bali M, Lemster T, and Akabas MH (2005) A Role for the β1-β2 loop in the gating of 5-HT3 receptors. *J Neurosci* **25:**9358–9366.

Revah F, Bertrand D, Galzi JL, Devillers-Thiery A, Mulle C, Hussy N, Bertrand S, Ballivet M, and Changeux JP (1991) Mutations in the channel domain alter desensitization of a neuronal nicotinic receptor. *Nature (Lond)* **353:**846–849.

Sala F, Mulet J, Sala S, Gerber S, and Criado M (2005) Charged amino acids of the N-terminal domain are involved in coupling binding and gating of α7 nicotinic receptors. *J Biol Chem* **280:**6642–6647.

Sine SM (2002) The nicotinic receptor ligand binding domain. *J Neurobiol* **53:**431–446.

Sine SM and Engel AG (2006) Recent advances in Cys-loop receptor structure and function. *Nature (Lond)* **440:**448–455.

Sine SM, Wang HL, and Bren N (2002) Lysine scanning mutagenesis delineates structural model of the nicotinic receptor ligand binding domain. *J Biol Chem* **277:**29210–29223.

Taly A, Delarue M, Grutter T, Nilges M, Le Novere N, Corringer PJ, and Changeux JP (2005) Normal mode analysis suggests a quaternary twist model for the nicotinic receptor gating mechanism. *Biophys J* **88:**3954–3965.

Unwin N (1993) Nicotinic acetylcholine receptor at 9 A resolution. *J Mol Biol* **229:**1101–1124.

Unwin N (2005) Refined structure of the nicotinic acetylcholine receptor at 4A resolution. *J Mol Biol* **346:**967–989.

Unwin N, Miyazawa A, Li J, and Fujiyoshi Y (2002) Activation of the nicotinic acetylcholine receptor involves a switch in conformation of the alpha subunits. *J Mol Biol* **319:**1165–1176.

Xie Y and Cohen JB (2001) Contributions of *Torpedo* nicotinic acetylcholine receptor gamma Trp-55 and delta Trp-57 to agonist and competitive antagonist function. *J Biol Chem* **276:**2417–2426.

Xiu X, Hanek AP, Wang J, Lester HA, and Dougherty DA (2005) A unified view of the role of electrostatic interactions in modulating the gating of cys loop receptors. *J Biol Chem* **280:**41655–41666.

Address correspondence to: Dr. Robert L. Rosenberg, Department of Pharmacology, CB# 7365, University of North Carolina at Chapel Hill, Chapel Hill, NC 27599-7365. E-mail: robert_rosenberg@med.unc.edu